Heliyon 9 (2023) e15689

Contents lists available at ScienceDirect

Heliyon

journal homepage: www.cell.com/heliyon

Research article

Application of silver nanoparticles for improving motor recovery after spinal cord injury via reduction of pro-inflammatory M1 macrophages

Jie Lin [a,b], Peikai Chen [a], Zhijia Tan [a], Yi Sun [c], Wai Kit Tam [b], Di Ao [b], Wei Shen [b], Victor Yu-Leong Leung [b,***], Kenneth Man Chee Cheung [a,b,**], Michael Kai Tsun To [a,b,*]

[a] *Department of Orthopaedics & Traumatology, The University of Hong Kong Shenzhen Hospital, School of Clinical Medicine, The University of Hong Kong, Shenzhen, Guangdong, 518053, China*
[b] *Department of Orthopaedics & Traumatology, School of Clinical Medicine, The University of Hong Kong, 21 Sassoon Road, Pokfulam, Hong Kong SAR, China*
[c] *Department of Sports Medicine, Peking University-Shenzhen Hospital, Shenzhen, Guangdong, 518034, China*

A B S T R A C T

Silver nanoparticles (AgNPs) possess anti-inflammatory activities and have been widely deployed for promoting tissue repair. Here we explored the efficacy of AgNPs on functional recovery after spinal cord injury (SCI). Our data indicated that, in a SCI rat model, local AgNPs delivery could significantly recover locomotor function and exert neuroprotection through reducing of pro-inflammatory M1 survival. Furthermore, in comparison with Raw 264.7-derived M0 and M2, a higher level of AgNPs uptake and more pronounced cytotoxicity were detected in M1. RNA-seq analysis revealed the apoptotic genes in M1 were upregulated by AgNPs, whereas in M0 and M2, pro-apoptotic genes were downregulated and PI3k-Akt pathway signaling pathway was upregulated. Moreover, AgNPs treatment preferentially reduced cell viability of human monocyte-derived M1 comparing to M2, supporting its effect on M1 in human. Overall, our findings reveal AgNPs could suppress M1 activity and imply its therapeutic potential in promoting post-SCI motor recovery.

1. Introduction

Silver nanoparticles (AgNPs) are silver particles at Nano scale ranging from 1 nm to 100 nm. Due to their antimicrobial and anti-inflammatory features, AgNPs have been widely utilized in many medical fields, including clinical diagnosis, drug delivery and medical production [1–3]. AgNPs also show a capacity in promoting tissue regeneration, yet the mechanism is not well understood [4–7]. Our group previously reported that AgNPs could promote wound healing, tendon repairing, and bone fracture healing in part through alleviation of tumor necrosis factor alpha (TNFα) expression [8–10]. We reasoned that AgNPs may have a potential in promoting functional recovery in other injury models through regulation of inflammation.

* Corresponding author. Department of Orthopaedics & Traumatology, The University of Hong Kong Shenzhen Hospital, School of Clinical Medicine, The University of Hong Kong, Shenzhen, Guangdong, 518053, China
** Corresponding author. Department of Orthopaedics & Traumatology, The University of Hong Kong Shenzhen Hospital, School of Clinical Medicine, The University of Hong Kong, Shenzhen, Guangdong, 518053, China
*** Corresponding author. Department of Orthopaedics & Traumatology, School of Clinical Medicine, The University of Hong Kong, 21 Sassoon Road, Pokfulam, Hong Kong SAR, China
E-mail addresses: vicleung@hku.hk (V.Y.-L. Leung), cheungmc@hku.hk (K.M.C. Cheung), duqj@hku-szh.org, mikektto@hku.hk (M.K.T. To).

https://doi.org/10.1016/j.heliyon.2023.e15689
Received 14 March 2023; Received in revised form 16 April 2023; Accepted 19 April 2023
Available online 9 May 2023

Spinal cord injury (SCI) leads to severe functional deficits or even death. SCI is commonly resulted from trauma, in particular traffic accidents and falls from height. Spine disorders or surgeries may also cause SCI. Tissue injury triggers inflammatory response to prompt clearance of apoptotic or necrotic cells, which is crucial for tissue repair. In the acute phase (the first 48 h), macrophages, as main cells with relatively long period of existence could be activated into pro-inflammatory M1 and anti-inflammatory M2 with distinct function in the tissue repair process [11–13]. Classically activated M1 macrophages are characterized by higher level of pro-inflammatory mediators such as iNOS (inducible nitric oxide synthase), IL-1β, IFNγ and TNFα to amplify inflammatory reaction [14]. Contrarily, alternatively activated M2 macrophage highly produce factors such as Arginase 1 (Arg1), CD206 and IL10 that locomotor recovery were critically dependent on [15,16]. A balance of pro- and anti-inflammatory activities is required for clearance of pathogenic antigens and enabling functional recovery [17]. In SCI, dysfunction of inflammatory response can initiate incidental secondary injury cascade in the form of hemorrhage, edema and ischemia to exacerbate epicentre. Secondary injury is destructive and further causes cell death and functional disabilities. It is well acknowledged that resolution of secondary injury, including a reduction of pro-inflammatory M1 or inhibiting the expression of M1 markers contributes to functional recovery. The efficacy and safety of methylprednisolone (MPS), the standard clinical treatment for SCI patients, have been challenged, as previous studies demonstrated that it could result in severe complications, including changes in metabolism and high risks of fatality [18,19]. As a neuroprotective

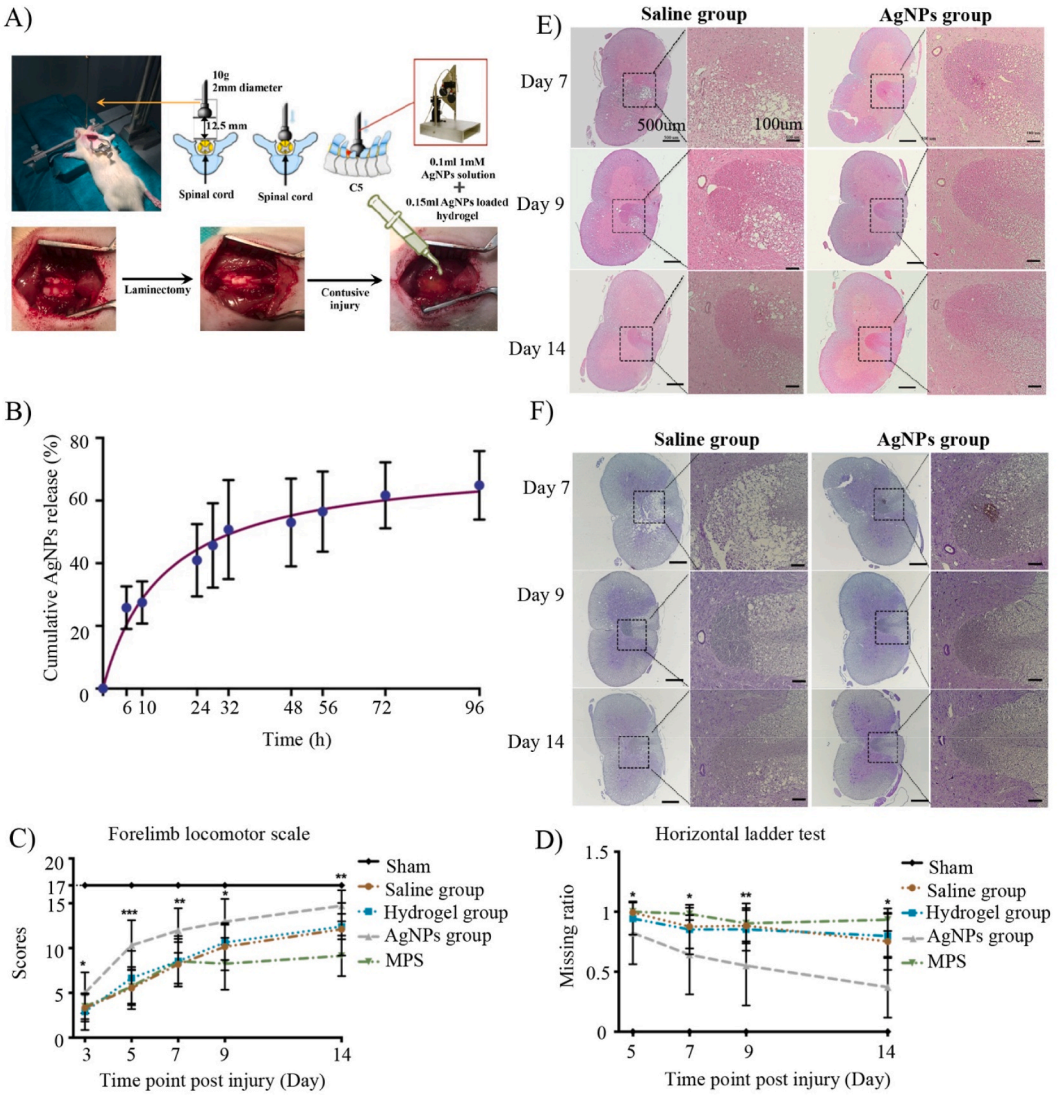

Fig. 1. AgNPs improved functional recovery and protected injured spinal cord after SCI. A) Surgical workflow of animal model; B)AgNPs release profile of HAMC hydrogel at 37° and composition. C, D)Functional restoration was evaluated with FLS and horizontal ladder test. 118 SD Rats in total: sham group (n = 20), saline group (n = 20), hydrogel group (n = 27), AgNPs group (n = 30), MPS group (n = 21); Representative images of H&E staining (E) and Luxol fast blue staining (F) to assess vacuolization and demyelination (scale bars = 500 μm, scale bars in the higher magnification images are 500 μm). (For interpretation of the references to colour in this figure legend, the reader is referred to the Web version of this article.)

drug, Riluzole provides an alternative therapeutic strategy for SCI, although the timing and dosage remains controversial. Therefore, there remains a pressing necessity to recruit more efficient therapeutics.

To date, the inflammatory response and functional recovery resulted from AgNPs treatment remains unclear. In this study, we hypothesized that AgNPs could inhibit inflammatory response and promote motor recovery after SCI. Firstly, we utilized a rat contusion model of SCI to examine the effects of AgNPs on regulating inflammation and early motor recovery at the acute phase. We studied locomotor outcomes using behavioural tests and conducted histological analysis to examine M1 and M2 macrophage activities at the injury site. An *in vitro* study with Raw 264.7-derived macrophage subtypes were performed to investigate the cytotoxicity and internalization of AgNPs as well as the impact of AgNPs on iNOS expression. Transcriptomic analysis was also conducted to reveal the potential molecular mechanisms of the interaction between AgNPs and macrophage subtypes. Moreover, human blood monocytes were utilized to investigate whether AgNPs were potent agents to suppress inflammation for clinical treatment in future.

2. Results

2.1. AgNPs improved locomotor function and ameliorated injury site after SCI

AgNPs were synthesized in chemical approaches and characterized by TEM (Fig. S1a, S1b), showing a size of around 10 nm. Owing

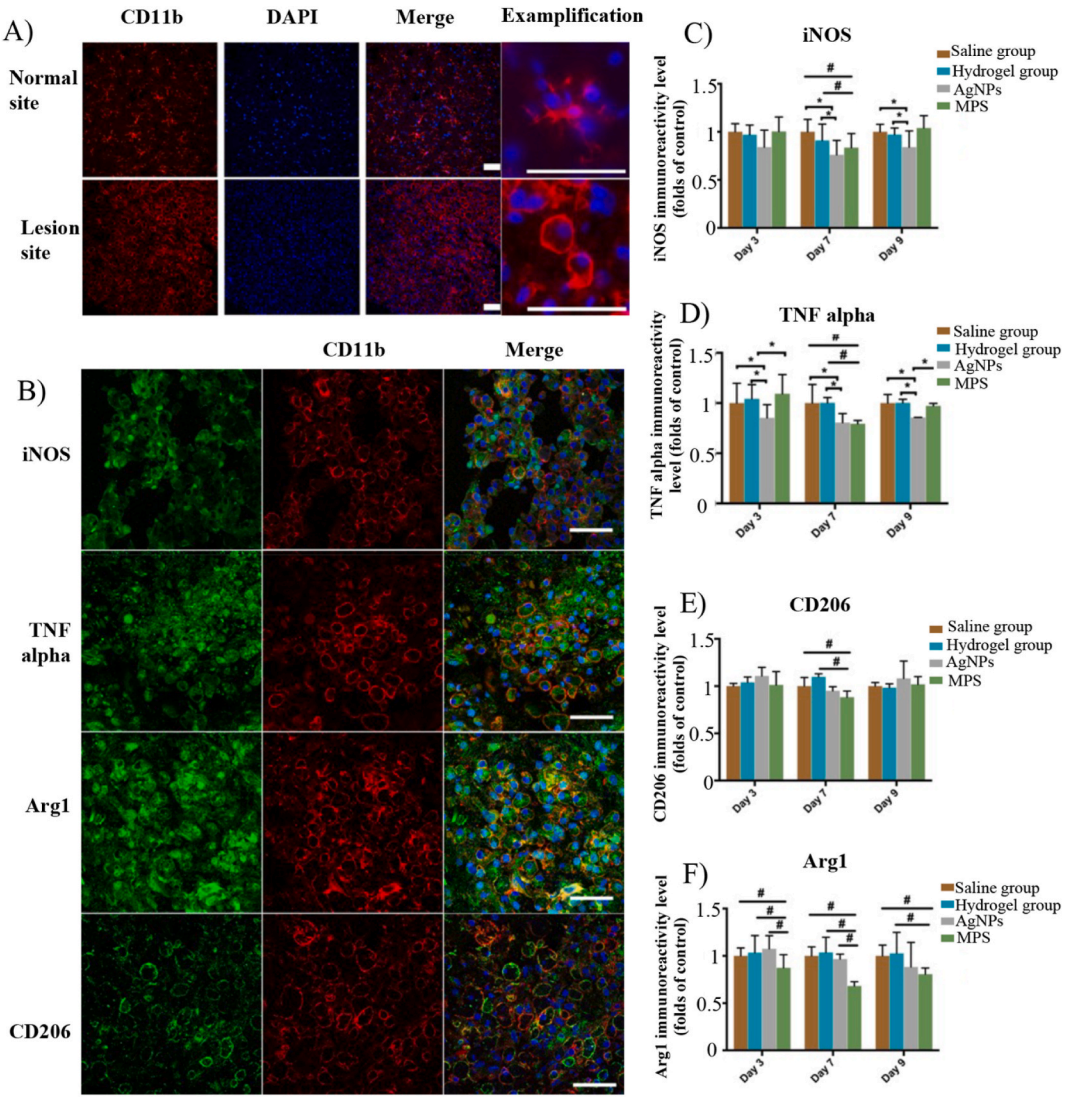

Fig. 2. AgNPs suppressed pro-inflammatory M1 at the injury site. A) Immunofluorescence examination of CD11b + macrophages at the normal site and injured site. Scale bars represent 50 μm; B) Morphologic characterization of M1 (TNF alpha, iNOS) and M2 (Arg1, CD206) at the lesion site. Scale bars = 50 μm; C, D, E, F) Immunofluorescence quantification for M1 and M2 at activated-CD11b positive area by custom script: (n = 3–5) in each group at different time point.

to thermal sensitivity and absorbent capacity, HAMC hydrogel composing of hyaluronic acid and methyl cellulose was applied as a vehicle of AgNPs [20]. Study of cumulative release of AgNPs from HAMC hydrogel (Fig. 1B) showed 41.6% and 53% AgNPs release from hydrogel in 24 h and 48 h respectively. However, a low amount of AgNPs release (13%) was observed from 48 h to 96 h. This indicated the hydrogel system could support gradual release of AgNPs over 48 h.

Considering the importance of hand function in life independence and quality, hand function recovery is regarded as the first priority in SCI patients [21]. In present study, a rat model of ipsilateral forelimb injury resulted from unilateral laminectomy on cervical level was employed (Fig. 1A) [22]. Forelimb locomotor scale (FLS) in combination with horizontal ladder test were used to examine the sequential locomotor recovery of affected limb as well as coordinated motor function after contusion injury [23]. In the FLS test, animals with better motor function gained higher scores. Rats in the hydrogel group showed motor function comparable to the saline group (Fig. 1C). Interestingly, the AgNPs group showed higher scores at all time points (FLS score from 5.0, 10.3, 12.0, 12.9 to 14.7). Compared to the hydrogel group, MPS group displayed the same level of locomotor deficits on day 3, 5 and 7 and the level was maintained on day 9 and 14. In horizontal ladder walking test, animals in hydrogel group displayed missing ratios of 0.94, 0.85, 0.85, 0.80 from day 5 to day 14. MPS group showed lower missing ratio on day 7 and day 9. In contrast, AgNPs group showed remarkably reduced missing ratios at all time points (Fig. 1D). Altogether, both FLS and horizontal ladder walking tests indicated AgNPs promoted motor recovery after SCI.

Given the enhanced motor recovery, histological analysis was conducted to examine whether AgNPs treatment modified the lesion site remodelling or healing. H&E staining revealed a damaged spinal cord in both the saline group and the AgNPs group. However, smaller vacuoles were observed in the AgNPs group compared with the saline group, implying reduced neuron destruction (Fig. 1E). Because neuron loss and degeneration could lead to demyelination, the extent of demyelination in the spinal cord was examined by Luxol fast blue staining. At day 7, 9 and 14, higher intensity of violet colour, which indicates myelin expression, was detected in the AgNPs group than in the saline group, suggesting less demyelination in the AgNPs group (Fig. 1F). Altogether, these findings suggested

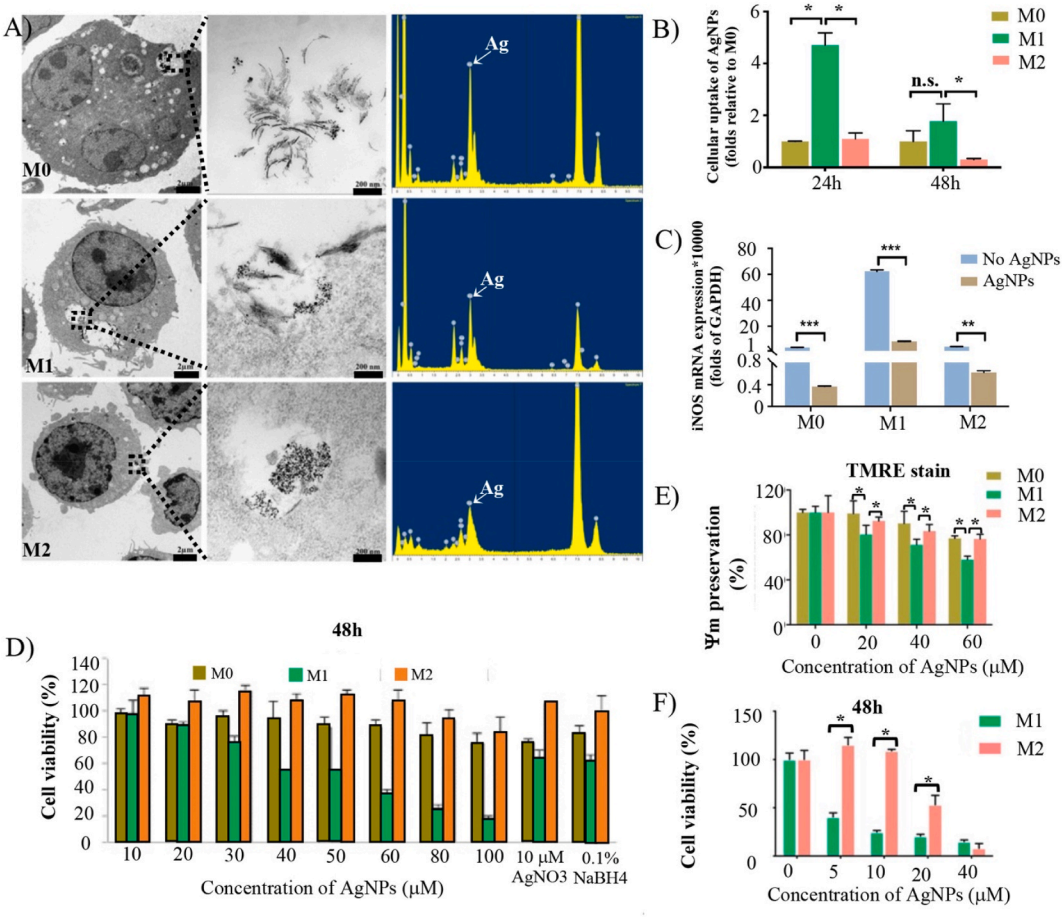

Fig. 3. A) TEM images for M0, M1 and M2 after exposure to 60 μM AgNPs for 48 h (scale bar = 2 μm, scale bar in higher magnification represents 200 nm). EDS spectrum corresponding to each group shown the presence of Ag; B) ICP-MS measurement of AgNPs uptake in M0, M1 and M2 at 24 h and 48 h;Cc) Effect of AgNPs on iNOS expression at mRNA level in M0, M1 and M2. Data were normalized to GAPDH and represented relative mRNA level of iNOS; D) Cytotoxicity of AgNPs on Raw 264.7- derived M0, M1 and M2 via MTT assay; E) Early apoptosis assessment via TMRE stain; f) Cytotoxicity of AgNPs on human monocytes-derived M1 and M2. M1 and M2 were incubated with AgNPs at different concentrations for 48 h.

A)

(Folds>2, p<0.05)	Upregulated DEGs	Downregulated DEGs
AgNPs-treated M0 vs M0	211	60
AgNPs-treated M1 vs M1	91	53
AgNPs-treated M2 vs M2	219	63

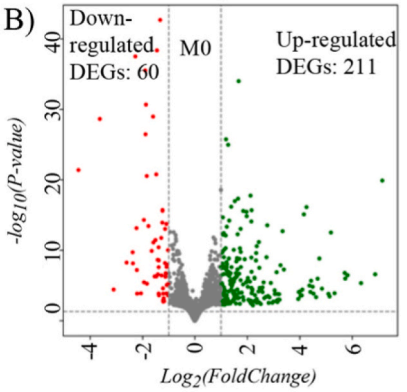

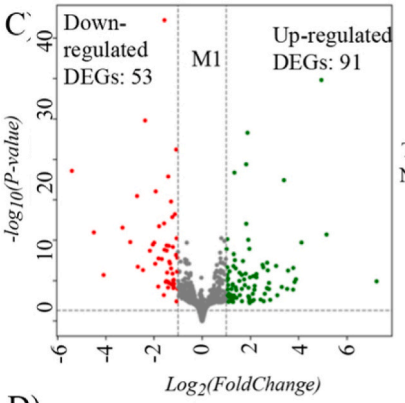

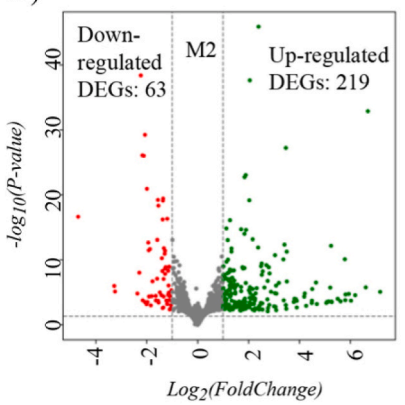

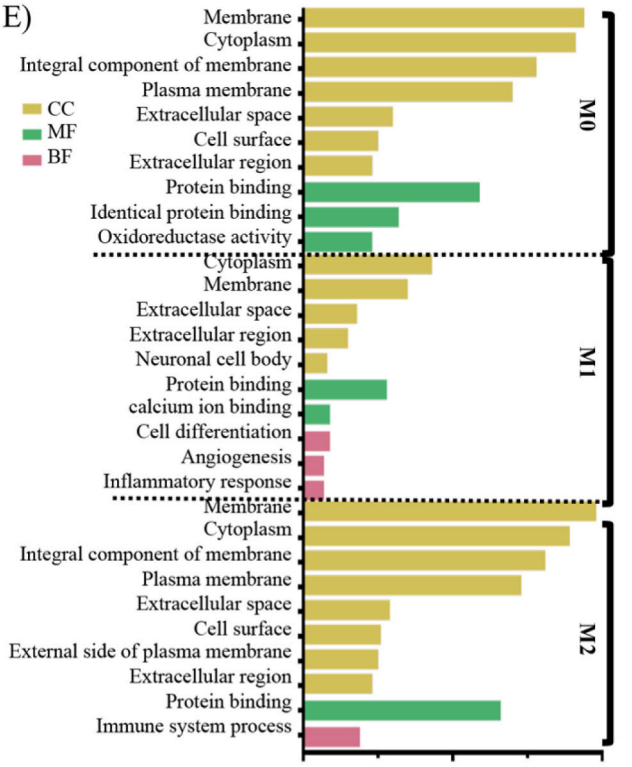

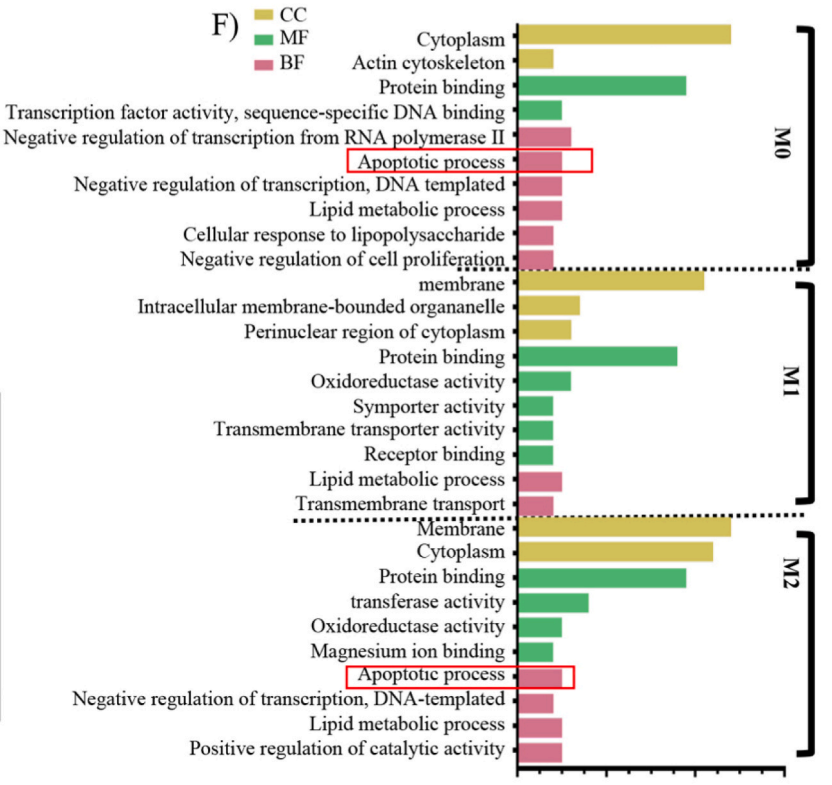

(caption on next page)

Fig. 4. A) Upregulated DEGs and downregulated DEGs in M0, M1 and M2 respectively after AgNPs treatment; B, C, D) Volcano plots shown downregulated DEGs and upregulated DEGs in M0, M1 and M2 with treatment of AgNPs. Induction of pro-apoptotic DEGs (Fabp4, Col15a1, Cxcl14 and Slc8a1) in AgNPs treated-M1 were detected from upregulated DEGs in C); GO analysis on E) upregulated DEGs and F) downregulated DEGs in AgNPs-treated M0, AgNPs-treated M1 as well as AgNPs-treated M2.

that AgNPs treatment could exhibit neuroprotection in SCI.

By immunostaining, macrophage marker CD11b showed ramified or amoeboid expression patterns in the normal spinal cord but a strong membrane expression after injury (Fig. 2A). Morphology of Arg1, CD206, TNF alpha and iNOS were subsequently showed (Fig. 2B). Compared with the saline group, M1 markers iNOS and TNF alpha in the hydrogel group exhibited a similar level of expression (Fig. 2B). AgNPs group displayed a downregulation of iNOS and TNF alpha at all time points. iNOS and TNF alpha production in MPS group were also reduced at day 7 (Fig. 2C and D). Expression of M2 macrophage markers in hydrogel group showed no significant changes (Fig. 2E and F). However, MPS significantly inhibited the expression of Arg1 on day 3, 7 and 9 as well as CD206 on day 7, which suggested that MPS can not only impact on the pro-inflammatory M1 but also the beneficial M2.

2.2. *Preferential AgNPs internalization and cytotoxicity in M1 macrophages*

Monocytes (Raw 264.7) with exposure to LPS plus IFN gamma or IL-4 could be polarized into M1 and M2 respectively [24,25]. Macrophage subtypes were characterized by the expression of M1 markers (iNOS, TNF alpha) and M2 markers (Arg1, IL-10) at the mRNA level (Fig. S4) [26–29]. TEM and ICP-MS analysis were conducted to estimate the AgNPs uptake capacity in M0, M1 and M2. TEM micrographs revealed AgNPs could be located within the cytoplasm 48 h after treatment (Fig. 3A). Specific AgNPs-containing organelles were not observed. EDS spectroscopy validated the internalized element as Ag. ICP-MS results showed that at 24 h concentration of AgNPs in M2 was at a similar level to M0, whereas five folds of AgNPs concentration was observed in M1 compared to M0 and M2. At 48 h, AgNPs concentration in M1 was also higher (1.78 folds) than in M0. M2 accumulated only a third of the concentration in M0 (Fig. 3B). A higher capacity of AgNPs uptake in M1 is consistent with previous studies showing that IL-4 polarized M2 macrophages displayed mitigated phagocytosis [30,31]. To investigate if AgNPs suppressed pro-inflammatory effect, iNOS production was quantified in AgNPs treated-M0, M1 and M2. qRT-PCR data demonstrated that iNOS expression was significantly downregulated in M0, M1 and M2 (Fig. 3C). AgNPs are reported to induce cell apoptosis after internalization. Therefore, we postulated that M1 macrophages were more sensitive to the cytotoxicity of AgNPs than M0 and M2 due to their high capacity of AgNPs uptake. To examine toxicity of AgNPs in macrophage subtypes, MTT assay was accordingly performed. With treatment of AgNPs at concentrations less than 60 μM for 48 h, cell viability of M0 and M2 were hardly or lightly affected in MTT assay. However, AgNPs induced remarkably lower

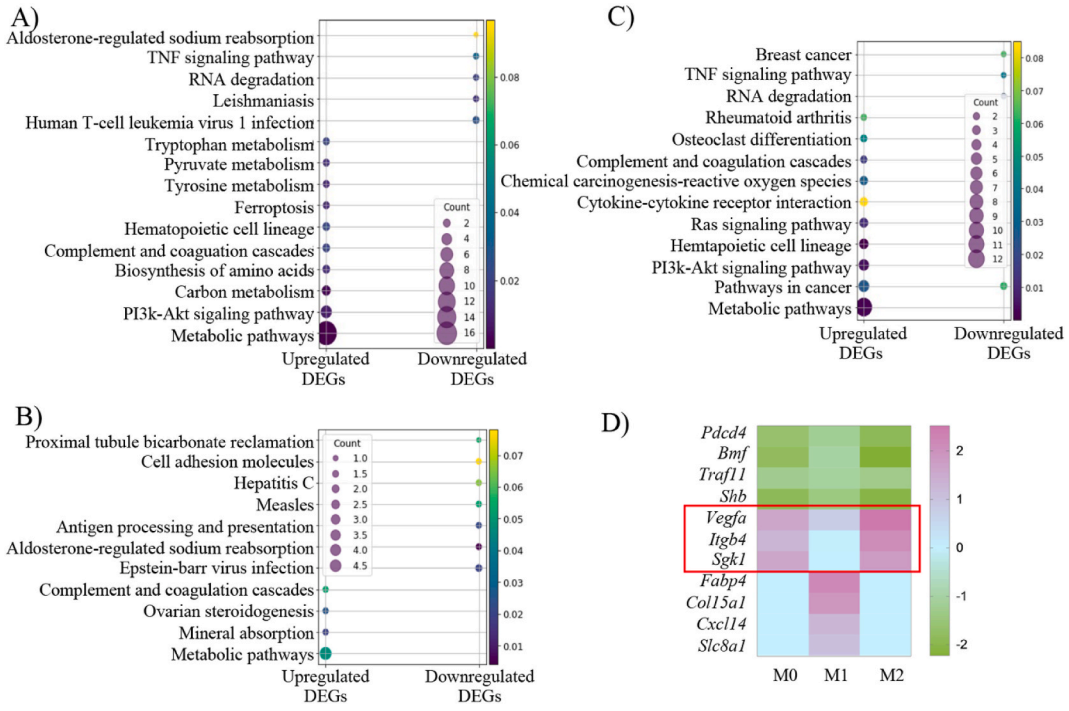

Fig. 5. KEGG bioinformatics analysis determined pathways associated to the upregulated and downregulated DEGs in A) M0, B) M1 and C) M2 after treatment of AgNPs; D) Heatmap of DEGs related to pro-apoptosis and anti-apoptosis (highlighted in red line) in M0, M1 and M2. (For interpretation of the references to colour in this figure legend, the reader is referred to the Web version of this article.)

cell viability in M1, implying that AgNPs is more cytotoxic to M1 than M0 and M2 (Fig. 3D). PI stain shown AgNPs cannot result in cell cycle arrest (Fig. S5). TMRE staining was subsequently used to further assess early apoptosis. With increasing AgNPs concentrations, mitochondrial membrane potential (Ψm) gradually decreased in M0, M1 and M2 due to defective depolarization of Ψm (Fig. 3E). However, a stronger Ψm reduction in M1 comparing with M0 and M2 was observed, implying more significant apoptosis in M1.

To examine if AgNPs could be applied for clinical translation, effect of AgNPs was examined in human blood monocytes derived-M1 and M2 macrophages (Fig. S6). Cytotoxicity assay showed that AgNPs at increasing concentrations resulted in more M1 death and M2. However, AgNPs at the same different concentration caused a lower cell viability in M1 than in M2 at 48 h (Fig. 3F), suggesting that AgNPs may potentially inhibit pro-inflammatory M1 in human.

2.3. AgNPs increased the expression of apoptotic DEGs (differentially expressed genes) in M1

The molecular mechanisms of AgNPs in regulation of pro-apoptotic events in M0, M1 and M2 macrophages were studied by RNA-seq analysis. Differentially expressed genes (DEGs) were defined (fold changes >2, $p < 0.05$) in AgNPs-treated M0 versus M0, AgNPs-treated-M1 versus M1 and AgNPs-treated M2 versus M2. The volcano plot illustrates 91 upregulated DEGs and 53 down-regulated DEGs in M1 after AgNPs treatment (Fig. 4A and C). Upregulated genes (*Fabp4, Col15a1, Cxcl14* and *Slc8a1*) associated to cell apoptosis were detected in M1. These upregulated DEGs implied AgNPs triggered apoptosis in M1 [32–35]. Moreover, we also observed that AgNPs resulted in 211 upregulated DEGs and 60 downregulated DEGs in M0, as well as 219 upregulated DEGs and 63 downregulated DEGs in M2 (Fig. 4A, B and 4D). The upregulated DEGs or downregulated DEGs were subjected to Gene Ontology (GO) database analysis. DEGs were typically divided into three functional categories: cellular component (CC), molecular function (MF) and biological process (BP), and the top 10 enriched terms were identified (Fig. 4E and F). Results showed that apoptotic process was enriched with downregulation of the DEGs in M0 and M2. However, inhibition of apoptotic genes (*Pdcd4, Bmf, Traf1* and *Shb*) enriched in apoptotic process were demonstrated to reduce apoptosis in many literatures [36–40]. Therefore, the lower expression of apoptotic genes in AgNPs-treated M0 and AgNPs-treated M2 suggested that AgNPs might protect M0 and M2 macrophages against apoptosis.

The Kyoto Encyclopedia of Genes and Genomes (KEGG) pathway for cellular process and signaling was analyzed. The top KEGG pathways were displayed in Fig. 5A, B and 5C. Pathway enrichment revealed the that AgNPs upregulated PI3K-Akt signaling pathway in M0 and M2. It was reported that PI3K-Akt signaling pathway was involved in induction of anti-apoptotic regulation [41–43]. Upregulated genes *Vegfa, Itgb4* and *Sgk1* (Fig. 5d) in PI3K-Akt pathway were reported to be anti-apoptotic and could promote cell survival, indicating that these genes were potentially involved in protecting M0 and M2 against apoptosis after AgNPs treatment [44–47]. In summary, AgNPs treatment resulted in upregulation of pro-apoptotic DEGs in M1. However, pro-apoptotic genes were significantly inhibited, and anti-apoptotic genes were induced in M0 as well as M2 after AgNPs treatment (Fig. 5D).

3. Discussion

In this study, we discovered that AgNPs may exert cytotoxicity on M1 macrophages and ameliorate secondary damage of SCI with a positive impact on functional outcomes. This suggests a novel application of AgNPs for motor improvement in SCI via suppressing pro-inflammatory events and their potential for management of SCI patients.

SD rats with contusion injury at cervical level mimics the pathology of human SCI [22]. At the injury site, Our findings suggest AgNPs can mitigate the vacuolization and demyelination of neurons, and preferentially reduce M1 survival without significant impact on M2. Many studies indicate that inhibition of pro-inflammatory M1 can prevent necroptosis of oligodendrocytes which contributes to demyelination. For example, Fan et al. demonstrated that suppressing M1 macrophages via STAT1 and NF-kB signaling pathway reduced myelin loss [48]. Moreover, reduction of iNOS expression was documented to correlate with neuron survival and prevent lesion site from further damage [49,50]. Animals with iNOS deficiency or inhibition also accelerated motor recovery in long-term [23, 51]. Therefore, mitigation of neurodegeneration resulted from iNOS reduction contribute and less deleterious impact of M1 protected injury site against further damage. In addition, amelioration of secondary injury might provide M2 with a microenvironment favourable to repair. Moreover, our data show that MPS exhibited impaired locomotor function in FLS (on day 9, day 14) and horizontal ladder test (on day 7, day 14) when compared to the other groups, suggesting MPS may exert detrimental effects on both M1 and M2.

In consistent with the findings *in vivo*, our *in vitro* results suggest an impact of AgNPs on the fate of Raw 264.7 cells-derived M1 and M2 with AgNPs. We observed that AgNPs reduced iNOS production of both M1 and M2, implying an anti-inflammatory effect. Indeed, after differentiation of macrophages into M1 and M2 with inflammatory stimuli, genes that regulate inflammatory response or impact morphology re-programmed. These activated signaling cascades may result in distinct behavior of macrophage subtypes, such as the capacity of pathogen uptake. Although a body of literatures evidenced that M1 could uptake more pathogens than M2, the molecular mechanism remains unclear. In present study, we observed M1 phagocytized more AgNPs *in vitro*, and that AgNPs led to less cytotoxicity in M0 and M2 than M1. In the transcriptomics analysis, AgNPs treated M1 showed fewer DEGs (144 in total) compared with AgNPs treated M0 (271 in total) or M2 (282 in total). Of all the DEGs in M1, pro-apoptotic genes were significantly upregulated, implying AgNPs promoted apoptosis in M1 macrophages. However, in M0 and M2, AgNPs induced downregulation of DEGs involved in apoptotic process but upregulation of DEGs in the PI3k-Akt signaling pathway. PI3k-Akt signaling pathway in M0 and M2 protected cells against apoptosis. Therefore, these DEGs enriched in those protective pathways may be involved in the molecular mechanisms, underlying why AgNPs uptake caused less damage to M0 and M2 than in M1.

Spinal surgeries, including revision spinal surgery, could lead to neural damage. In this perspective, we postulate that AgNPs might serve as a neuroprotective agents and improve surgical outcomes if administrated during spinal operations. Despite the capacity of

AgNPs in promoting tissue recovery, their toxicity remains a concern and its safety has been debated. Previous studies indicated that the toxicity of AgNPs was dependent on dosage and cell type *in vitro* [52]. *In vivo* studies reported that AgNPs were mainly excreted via feces. However, rats with daily oral exposure to AgNPs (90 mg/kg) for 28 days exhibited silver retention in tissues including spleen, liver and kidney without hepatoxicity and immunotoxicity [53,54]. Another study investigated the toxicity of AgNPs *in vivo* at 30 mg/kg, 300 mg/kg and 1000 mg/kg AgNPs, and found no genotoxicity. Our study used a much lower concentration AgNPs (45 μg/kg) with local delivery at single dose without detectable accumulation in liver or kidney. The effects of dosage and administration approach should be explored in future.

4. Methods

4.1. Animal surgery

8 week-old Sprague–Dawley (SD) rats were obtained from the Laboratory Animal Unit, The University of Hong Kong (HKU). The experimental protocol was approved by the Committee of the Use of Live Animals in Teaching and Research, HKU (CULATR 3743-15). 118 rats were randomly distributed into sham group (n = 20), saline group (n = 20), hydrogel group (n = 27), AgNPs group (n = 30), MPS group (n = 21). Laminectomy was performed with microsurgery tools to expose the spinal cord at C5 level. Subsequently, a customized weight-drop injury device modified from NYU impactor device was utilized to create NYU-MASCIS Contusion SCI at the left side of C5 level. Sham group were animals with exposure of spinal cord but no contusion injury. Post injury, AgNPs group received injection of 0.1 mL AgNPs solution plus 0.15 mL AgNP-loaded HAMC hydrogel. Saline group and hydrogel group were injected by saline and HAMC hydrogel plus saline at the injury site respectively. MPS group were injected MPS (30 mg/kg) intra-peritoneally. Surgery workflow was shown in Fig. 1A.

4.2. Preparation of hydrogel and release profile

Briefly, 5 wt% methylcellulose (MC; Sigma-Aldrich) and 2 wt% sodium hyaluronate (HA; Ryon) were sequentially dispersed in artificial cerebrospinal fluid (aCSF) at 60 °C and allowed to dissolve at 4 °C overnight. Additionally, AgNPs-loaded HAMC hydrogel were fabricated by distributing 5 wt% MC and 2 wt% HA into AgNPs solution and dissolving at 4 °C overnight. Cumulative release profile of AgNPs from HAMC hydrogel was measured at a serial of time periods. Specifically, AgNPs-loaded hydrogel pieces (1 g) were stored in aCSF (10 mL) and allowed to oscillate at a frequency of 60 rpm in a rotary shaker at 37 °C. At various time points, 0.5 mL releasing medium was extracted and the amount of AgNPs released was measured by optical density at max (400 nm), using spectrophotometer (NanoDrop 2000; Thermo Scientific).

4.3. Histology

Injured segments of spinal cord were harvested and fixed in the 4% PFA overnight. After dehydration, the tissue pieces were embedded within paraffin. 6-μm paraffin embedded transverse sections of injured spinal cord tissue were prepared. For H&E staining, slides were immersed in hematoxylin (Sigma-Aldrich) for 5 min, followed by washing in running tap water for 5 min and distilled water (5 min). Slides were then stained in Eosin (30 s) and dehydrated in alcohol solution (95% ethanol, 100% ethanol) and xylene. Samples were mounted with xylene. In Luxol fast blue staining, spinal cord sections were incubated with luxol fast blue solution overnight in 56 °C degree over, washed in 95% alcohol and distilled water, differentiated in the lithium carbonate solution and 70% alcohol for 30 s. After washing in distilled water, slides were counterstained in cresyl violet solution for 30–40 s. Subsequently, slides were processed by 95% alcohol for 5 min, 100% alcohol and xylene for 5 min twice, mounted by resinous medium. Signals were examined and recorded under Nikon fluorescent microscope (Nikon E800).

4.4. Behavioural tests

Rats were placed in an enclosure (5 cm × 1 m) allowing free movements. The categories of scoring system in FLS test were based on behavioural changes observed after unilateral cervical injury, with range from 0 (complete paralysis) to 17 (healthy condition) [23]. In horizontal ladder test, the animals were offered a task to reach their home cage by crossing a horizontally-placed ladder with metal rungs (3 mm diameter) randomly. In each trial, at least 10 steps were recorded. Any kind of foot slips or total misses was defined as miss. Missing ratio was calculated by number of missing steps/10 steps in one trial. The mean numbers of error steps for 5 trials was calculated for comparison. Each rat performed the test trials by 3 times at each time point after 1 or 2 warming-up practices. All the rats' performances on the behavior were recorded by digital videos for further analysis by two blinded observers.

4.5. Immunofluorescence

For immunohistochemistry staining, fixed spinal cord tissues were dehydrated in 30% glucose solution at 4° freezer overnight, followed by embedding in OCT compound and sectioning at 15 μm thickness by cryotome. Transverse sections were washed by PBS and subsequently incubated in 1% BSA. Sections were incubated with antibody against iNOS (Gene Tex, GTX74171), TNF alpha (Abcam), Arg1 (Cell signaling, 93,688), CD206 (Abcam, ab64693), or CD11b (Bio-rad, MCA275R) at 4° overnight, followed by secondary antibodies (Gene Tex). Sections were mounted in mounting medium with DAPI(Vector) to visualize the nuclei.

4.6. Cell culture

Raw 264.7 cells were cultured in Dulbecco's Modified Eagle Medium (DMEM) medium supplemented with 10% FBS, 100 U/ml penicillin, 100 μg/mL streptomycin) at 37 °C, 5% CO_2. LPS (100 ng/mL) plus IFNγ ((2.5 ng/mL) or IL-4 (10 ng/mL) were added to polarize the cells into M1 and M2 for 12 h. Human blood monocytes derived-M1 and M2 were cultured in complete RPMI 1640 medium, supplemented with 10% FBS, 100U/ml penicillin and streptomycin (100 μg/mL).

4.7. Quantitative RT-PCR

Total RNA of Raw 264.7-polarized M0, M1 and M2 were extracted by using RNeasy mini kit (Qiagen). The RNA concentration was determined by UV absorbance at the wavelength of 260 nm and 280 nm. Reverse transcription was conducted subsequently by primer script master mix (Takara). Amplification of cDNA (100 ng) was performed by utilizing SYBR green PCR master mix (Thermo Fisher Scientific) based on the manufacturer's instructions. All the primers were applied in the study were listed in the supplement (Table S1).

4.8. Transmission electron microscope (TEM) and energy-dispersive X-ray (EDS) analysis

In order to observe the internalization, M0, M1 and M2 were incubated in the media containing AgNPs for 24 h or 48 h. Then, cells were washed and fixed with 2.5% glutaraldehyde in cacodylate buffer overnight. After dehydration, embedding, being polarized and being cut into ultra-thin sections, the specific location of AgNPs in M0, M1 and M2 was examined under the transmission electron microscope. EDS analysis was applied for identification of elemental composition.

4.9. Inductively coupled plasma mass spectrometry (ICP-MS) assay

Firstly, M0, M1 and M2 were treated with AgNPs for 24 or 48 h. After cell counting and centrifugation, the precipitations were digested with concentrated HNO_3 and then diluted with deionized H_2O. The concentration of silver ions in M0, M1 and M2 was measured by ICP-MS after which the uptake amount of AgNPs in M0, M1 and M2 was calculated.

4.10. MTT (3-(4,5-dimethylthiazol-2-yl)-2,5-diphenyltetrazolium bromide) assay

Raw 264.7 cells were seeded onto a 96-well plate at the density of 1000 cells. After polarization, M0, M1 and M2 were incubated with different concentrations of AgNPs (10, 20, 30, 40, 50, 60, 80, 100 μM) for 2 days. MTT solution (5 mg/mL) was subsequently added for 3 h at 37 °C. After removing DMEM supernatant, 200 μl DMSO was added to dissolve purple precipitates. Absorbance was measured at 570 nm and 690 nm by using the microplate spectrophotometer.

4.11. TMRE stain

M0, M1 and M2 macrophage were cultured with AgNPs for 2 days. Following that, TMRE stain (Abcam) was conducted as manufacture's instruction. TMRE fluorescence intensity could be detected at emission wavelength 575 nm via microplate reader with excitation wavelength 549 nm.

4.12. Differentiation of human monocytes from healthy human blood into M1 and M2

The Institutional Review Board (IRB) of HKU/HA HKW approved all the experiments of human blood use in this study (IRB number: UW20-653). Human primary cells were isolated from fresh human blood donated by volunteers. Human lymphocytes were obtained from human blood through density centrifugation by using Ficoll-Paque plus (GE Healthcare). Then monocytes were isolated from lymphocytes by using CD14 microbeads (Miltenyi Biotech) according to manufacturer's instruction. The obtained monocytes were identified by using CD14 antibody (BD biosciences) via flow cytometry. For M1 differentiation, monocytes were treated with GM-CSF (100 ng/mL, PeproTech) for 7 days, followed by treatment of LPS (10 ng/mL, Sigma-Aldrich) plus IFN gamma (20 ng/mL, PeproTech) for 24 h. For M2 differentiation, monocytes were treated with M-CSF (10 ng/mL, PeproTech) for 7 days, followed by incubation with IL-4 (20 ng/mL, R&D Systems) for 24 h. M1 and M2 were confirmed by using M1 marker CD86 (BD Bioscience) and M2 maker CD206 (BD Biosciences) through flow cytometry.

4.13. Cytotoxicity test of AgNPs on human derived-M1 and M2

Human monocytes were seeded in 96-well plate with intensity of 10,000 cells/well, followed by polarization into M1 and M2. Then M1 and M2 cells were treated with AgNPs of different concentrations (5, 10, 20, 40 μM) for 2 days. Assessment of cell toxicity was conducted via MTT assay.

4.14. Bulk RNA sequencing

Samples (Raw 264.7-derived M0, M1 and M2 treated with or without 60 μM AgNPs for 48 h) for bulk RNA sequencing were

subdivided into 6 groups, 3 biological repeats in each group. Total RNA was extracted using RNase mini kit. Samples with RNA integrity numbers more than 7.0 were utilized for sequencing. The Center for PanorOmic Sciences (CPOS), HKU created libraries and sequenced the samples (Illumina). Sequence reads were processed and FASTQ sequence reads were aligned to mouse Genome GRCm38 with STAR version 2.5.2 (https://github.com/alexdobin/STAR) at default settings. Quantification of expression was processed by RSEM version 1.2.31 (https://deweylab.github.io/RSEM/). Analysis of DEGs performed at FDR (false discovery rate) < 0.05 using EBSeq version 1.18.0 (http://bioconductor.org/packages/release/bioc/html/EBSeq.html).

4.15. Functional enrichment

GO terms and KEGG pathway were analyzed using DAVID (https://david.ncifcrf.gov/).

4.16. Statistical analysis

Data were analyzed by one-way ANOVA. Differences were considered statistically significant at $p < 0.05$. Values were presented as mean $\pm$ SD.

Author contribution statement

Jie Lin: Conceived and designed the experiments; Performed the experiments; Analyzed and interpreted the data; Wrote the paper.
Pei Kai Chen: Analyzed and interpreted the data; Wrote the paper.
Zhi Jia Tan: Analyzed and interpreted the data; Contributed reagents, materials, analysis tools or data; Wrote the paper.
Yi Sun, Wai Kit Tam, Di Ao, Wei Shen: Performed the experiments.
Victor Leung, Kenneth Man Chee Cheung, Michael Kai Tsun To: Conceived and designed the experiments; Contributed reagents, materials, analysis tools or data; Wrote the paper.

Funding statement

Grant is from Research Impact Fund (RIF) (Grant No.: R7072-18), supported by University Grants committee.

Data availability statement

Data will be made available on request.

Declaration of competing interest

The authors declare that they have no known competing financial interests or personal relationships that could have appeared to influence the work reported in this paper

Abbreviations

AgNPs	silver nanoparticles
SCI	spinal cord injury
TNFα	tumor necrosis factor alpha
iNOS	inducible nitric oxide synthase
IL-1β	interleukin 1β
IFNγ	interferon gamma
Arg1	Arginase 1
CD206	macrophage mannose receptor
IL10	interleukin 10
MPS	methylprednisolone
SD	Sprague–Dawley
HAMC hydrogel	hyaluronic acid-methylcellulose hydrogel
aCSF	artificial cerebral spinal fluid
PFA	Paraformaldehyde
H&E	hematoxylin and eosin
FLS	forelimb locomotor scaling
IL-4	interleukin 4
DMEM	Dulbecco's Modified Eagle Medium
ICP-MS	Inductively coupled plasma mass spectrometry
MTT	(3-(4,5-Dimethylthiazol-2-yl)-2,5-Diphenyltetrazolium Bromide)
GM-CSF	Granulocyte macrophage colony-stimulating factor

M-CSF	Macrophage colony-stimulating factor
CD86	Cluster of Differentiation 8
TEM	Transmission electron microscopy
TMRE	Tetramethylrhodamine, Ethyl Ester
DEGs	differentially expressed genes
CC	cellular component
MF	molecular function
BP	biological process
KEGG	Kyoto Encyclopedia of Genes and Genomes
GO	gene ontology

References

[1] Z. Abbasi, S. Feizi, E. Taghipour, P. Ghadam, Green synthesis of silver nanoparticles using aqueous extract of dried Juglans regia green husk and examination of its biological properties, Green Process. Synth. 6 (5) (2017) 477–485.

[2] A. Hernández-Arteaga, J.d.J.Z. Nava, E.S. Kolosovas-Machuca, J.J. Velázquez-Salazar, E. Vinogradova, M. José-Yacamán, H.R. Navarro-Contreras, Diagnosis of breast cancer by analysis of sialic acid concentrations in human saliva by surface-enhanced Raman spectroscopy of silver nanoparticles, Nano Res. 10 (11) (2017) 3662–3670.

[3] L. Qiu, J.-W. Li, C.-Y. Hong, C.-Y. Pan, Silver nanoparticles covered with pH-sensitive camptothecin-loaded polymer prodrugs: switchable fluorescence "off" or "on" and drug delivery dynamics in living cells, ACS Appl. Mater. Interfaces 9 (46) (2017) 40887–40897.

[4] J. Tian, K.K.Y. Wong, C.-M. Ho, C.-N. Lok, W.-Y. Yu, C.-M. Che, J.-F. Chiu, P.K.H. Tam, Topical delivery of silver nanoparticles promotes wound healing, ChemMedChem 2 (1) (2007) 129–136.

[5] L. Deng, Y. Deng, K. Xie, AgNPs-decorated 3D printed PEEK implant for infection control and bone repair, Colloids Surf. B Biointerfaces 160 (2017) 483–492.

[6] B. Moldovan, L. David, A. Vulcu, L. Olenic, M. Perde-Schrepler, E. Fischer-Fodor, I. Baldea, S. Clichici, G.A. Filip, In vitro and in vivo anti-inflammatory properties of green synthesized silver nanoparticles using Viburnum opulus L. fruits extract, Mater. Sci. Eng. C Mater. Biol Appl. 79 (2017) 720–727.

[7] A. Oryan, E. Alemzadeh, J. Tashkhourian, S.F. Nami Ana, Topical delivery of chitosan-capped silver nanoparticles speeds up healing in burn wounds: a preclinical study, Carbohydr. Polym. 200 (2018) 82–92.

[8] K.H. Kwan, X. Liu, M.K. To, K.W. Yeung, C.-m. Ho, K.K. Wong, Modulation of collagen alignment by silver nanoparticles results in better mechanical properties in wound healing, Nanomed. Nanotechnol. Biol. Med. 7 (4) (2011) 497–504.

[9] K.H. Kwan, K.W. Yeung, X. Liu, K.K. Wong, H.C. Shum, Y.W. Lam, S.H. Cheng, K.M. Cheung, M.K. To, Silver nanoparticles alter proteoglycan expression in the promotion of tendon repair, Nanomed. Nanotechnol. Biol. Med. 10 (7) (2014) 1375–1383.

[10] R. Zhang, P. Lee, V.C. Lui, Y. Chen, X. Liu, C.N. Lok, M. To, K.W. Yeung, K.K. Wong, Silver nanoparticles promote osteogenesis of mesenchymal stem cells and improve bone fracture healing in osteogenesis mechanism mouse model, Nanomed. Nanotechnol. Biol. Med. 11 (8) (2015) 1949–1959.

[11] M. Schwartz, Macrophages and microglia in central nervous system injury: are they helpful or harmful? J. Cerebr. Blood Flow Metabol. 23 (4) (2003) 385.

[12] H. Prüss, M.A. Kopp, B. Brommer, N. Gatzemeier, I. Laginha, U. Dirnagl, J.M. Schwab, Non-Resolving aspects of acute inflammation after spinal cord injury (SCI): indices and resolution plateau, Brain Pathol. 21 (6) (2011) 652–660.

[13] T.M. Tsarouchas, D. Wehner, L. Cavone, T. Munir, M. Keatinge, M. Lambertus, A. Underhill, T. Barrett, E. Kassapis, N. Ogryzko, Dynamic control of proinflammatory cytokines Il-1β and Tnf-α by macrophages in zebrafish spinal cord regeneration, Nat. Commun. 9 (1) (2018) 1–17.

[14] K. Honjoh, H. Nakajima, T. Hirai, S. Watanabe, A. Matsumine, Relationship of inflammatory cytokines from M1-type microglia/macrophages at the injured site and lumbar enlargement with neuropathic pain after spinal cord injury in the CCL21 knockout (plt) mouse, Front. Cell. Neurosci. 13 (2019).

[15] J. Dalli, C.N. Serhan, Specific lipid mediator signatures of human phagocytes: microparticles stimulate macrophage efferocytosis and pro-resolving mediators, Blood 120 (15) (2012) e60–e72.

[16] R. Shechter, O. Miller, G. Yovel, N. Rosenzweig, A. London, J. Ruckh, K.-W. Kim, E. Klein, V. Kalchenko, P. Bendel, Sergio A. Lira, S. Jung, M. Schwartz, Recruitment of beneficial M2 macrophages to injured spinal cord is orchestrated by remote brain choroid plexus, Immunity 38 (3) (2013) 555–569.

[17] J.M. Cicchese, S. Evans, C. Hult, L.R. Joslyn, T. Wessler, J.A. Millar, S. Marino, N.A. Cilfone, J.T. Mattila, J.J. Linderman, D.E. Kirschner, Dynamic balance of pro- and anti-inflammatory signals controls disease and limits pathology, Immunol. Rev. 285 (1) (2018) 147–167.

[18] M.B. Bracken, W.F. Collins, D.F. Freeman, M.J. Shepard, F.W. Wagner, R.M. Silten, K.G. Hellenbrand, J. Ransohoff, W.E. Hunt, P.L. Perot, R.G. Grossman, B. A. Green, H.M. Eisenberg, N. Rifkinson, J.H. Goodman, J.N. Meagher, B. Fischer, G.L. Clifton, E.S. Flamm, S.E. Rawe, Efficacy of methylprednisolone in acute spinal cord injury, JAMA 251 (1) (1984) 45–52.

[19] S.H. Choi, C.-h. Sung, D.R. Heo, S.-Y. Jeong, C.-N. Kang, Incidence of acute spinal cord injury and associated complications of methylprednisolone therapy: a national population-based study in South Korea, Spinal Cord 58 (2) (2019) 232–237.

[20] A. Singh, L. Krisa, K.L. Frederick, H. Sandrow-Feinberg, S. Balasubramanian, S.K. Stackhouse, M. Murray, J.S. Shumsky, Forelimb locomotor rating scale for behavioral assessment of recovery after unilateral cervical spinal cord injury in rats, J. Neurosci. Methods 226 (2014) 124–131.

[21] D. Maggio, A. Singh, J. Iorgulescu, D. Bleicher, M. Ghosh, M. Lopez, L. Tuesta, D. Pearse, Identifying the long-term role of inducible nitric oxide synthase after contusive spinal cord injury using a transgenic mouse model, Int. J. Mol. Sci. 18 (2) (2017) 245.

[22] C. Lo, Y. Tran, K. Anderson, A. Craig, J. Middleton, Functional priorities in persons with spinal cord injury: using discrete choice experiments to determine preferences, J. Neurotrauma 33 (21) (2016) 1958–1968.

[23] Z. Huang, R. Li, J. Liu, Z. Huang, Y. Hu, X. Wu, Q. Zhu, Longitudinal electrophysiological changes after cervical hemi-contusion spinal cord injury in rats, Neurosci. Lett. 664 (2018) 116–122.

[24] A.K. Jha, S.C. Huang, A. Sergushichev, V. Lampropoulou, Y. Ivanova, E. Loginicheva, K. Chmielewski, K.M. Stewart, J. Ashall, B. Everts, E.J. Pearce, Network integration of parallel metabolic and transcriptional data reveals metabolic modules that regulate macrophage polarization, Immunity 42 (3) (2015) 419–430.

[25] C.P. Hans, Transcriptomics analysis reveals new insights into the roles of Notch1 signaling on macrophage polarization, Sci. Rep. 9 (1) (2019) 7999.

[26] J.P. Edwards, Biochemical and functional characterization of three activated macrophage populations, J. Leukoc. Biol. 80 (6) (2006) 1298.

[27] U.M. Gundra, N.M. Girgis, D. Ruckerl, S. Jenkins, L.N. Ward, Z.D. Kurtz, K.E. Wiens, M.S. Tang, U. Basu-Roy, A. Mansukhani, J.E. Allen, P.n. Loke, Alternatively activated macrophages derived from monocytes and tissue macrophages are phenotypically and functionally distinct, Blood 123 (20) (2014) e110–e122.

[28] J.W. Choi, Pyropia yezoensis glycoprotein promotes the M1 to M2 macrophage phenotypic switch via the STAT3 and STAT6 transcription factors, Int. J. Mol. Med. 38 (2) (2016) 666.

[29] G. Xu, Isomeranzin suppresses inflammation by inhibiting M1 macrophage polarization through the NF-κB and ERK pathway, Int. Immunopharm. 38 (2016) 175.

[30] A. Varin, S. Mukhopadhyay, G. Herbein, S. Gordon, Alternative activation of macrophages by IL-4 impairs phagocytosis of pathogens but potentiates microbial-induced signalling and cytokine secretion, Blood 115 (2) (2010) 353–362.

[31] Y. Qie, H. Yuan, C.A. von Roemeling, Y. Chen, X. Liu, K.D. Shih, J.A. Knight, H.W. Tun, R.E. Wharen, W. Jiang, B.Y.S. Kim, Surface modification of nanoparticles enables selective evasion of phagocytic clearance by distinct macrophage phenotypes, Sci. Rep. 6 (1) (2016) 26269.

[32] J.J. Muñoz, S.A. Drigo, M.C. Barros-Filho, F.A. Marchi, C. Scapulatempo-Neto, G.S. Pessoa, G.C. Guimarães, J.C.S. Trindade Filho, A. Lopes, M.A. Arruda, Down-regulation of SLC8A1 as a putative apoptosis evasion mechanism by modulation of calcium levels in penile carcinoma, J. Urol. 194 (1) (2015) 245–251.
[33] F. Sun, J. Du, H. Li, S. Hao, G. Zhao, F. Lu, FABP4 inhibitor BMS309403 protects against hypoxia-induced H9c2 cardiomyocyte apoptosis through attenuating endoplasmic reticulum stress, J. Cell Mol. Med. 24 (19) (2020) 11188–11197.
[34] J. Bi, Q. Liu, Y. Sun, X. Hu, X. He, C. Xu, CXCL14 inhibits the growth and promotes apoptosis of hepatocellular carcinoma cells via suppressing Akt/mTOR pathway, J. Recept. Signal Transduction 41 (6) (2021) 593–603.
[35] J. Cai, X. Wang, W. Liao, Y. Zhong, L. Chen, Z. Zhang, Silencing lncRNA 93358 inhibits the apoptosis of myocardial cells in myocardial infarction rats by inducing the expression of SLC8A1, BioMed Res. Int. 2022 (2022) 1138709–1138720.
[36] J. Dixelius, H. Larsson, T. Sasaki, K. Holmqvist, L. Lu, A.k. Engstrom, R. Timpl, M. Welsh, L. Claesson-Welsh, Endostatin-induced tyrosine kinase signaling through the Shb adaptor protein regulates endothelial cell apoptosis, Blood, J. Am. Soc. Hematol. 95 (11) (2000) 3403–3411.
[37] R. Hägerkvist, D. Mokhtari, C. Lindholm, F. Farnebo, G. Mostoslavsky, R.C. Mulligan, N. Welsh, M. Welsh, Consequences of Shb and c-Abl interactions for cell death in response to various stress stimuli, Exp. Cell Res. 313 (2) (2007) 284–291.
[38] F. Grespi, C. Soratroi, G. Krumschnabel, B. Sohm, C. Ploner, S. Geley, L. Hengst, G. Häcker, A. Villunger, BH3-only protein Bmf mediates apoptosis upon inhibition of CAP-dependent protein synthesis, Cell Death Differ. 17 (11) (2010) 1672–1683.
[39] R. Rajandram, N.C. Bennett, Z. Wang, J. Perry-Keene, D.A. Vesey, D.W. Johnson, G.C. Gobe, Patient samples of renal cell carcinoma show reduced expression of TRAF1 compared with normal kidney and functional studies in vitro indicate TRAF1 promotes apoptosis: potential for targeted therapy, Pathology 44 (5) (2012) 453–459.
[40] Z. Li, Y. Zhou, L. Zhang, K. Jia, S. Wang, M. Wang, N. Li, Y. Yu, X. Cao, J. Hou, microRNA-199a-3p inhibits hepatic apoptosis and hepatocarcinogenesis by targeting PDCD4, Oncogenesis 9 (10) (2020) 1–14.
[41] V.R. Babaev, J.D. Chew, L. Ding, S. Davis, M.D. Breyer, R.M. Breyer, J.A. Oates, S. Fazio, M.F. Linton, Macrophage EP4 deficiency increases apoptosis and suppresses early atherosclerosis, Cell Metabol. 8 (6) (2008) 492–501.
[42] P. Prieto, J. Cuenca, P.G. Través, M. Fernández-Velasco, P. Martín-Sanz, L. Boscá, Lipoxin A 4 impairment of apoptotic signaling in macrophages: implication of the PI3K/Akt and the ERK/Nrf-2 defense pathways, Cell Death Differ. 17 (7) (2010) 1179–1188.
[43] K. Volling, A. Thywissen, A.A. Brakhage, H.P. Saluz, Phagocytosis of melanized Aspergillus conidia by macrophages exerts cytoprotective effects by sustained PI3K/Akt signalling, Cell Microbiol. 13 (8) (2011) 1130–1148.
[44] T. Endo, M. Kusakabe, K. Sunadome, T. Yamamoto, E. Nishida, The kinase SGK1 in the endoderm and mesoderm promotes ectodermal survival by down-regulating components of the death-inducing signaling complex, Sci. Signal. 4 (156) (2011) ra2-ra2.
[45] J.D. Zhan, z. j. Yan, M.Y. Zhao, W.H. Qi, J. Lin, Z. Lin, Y.J. Huang, X.Y. Pan, X.H. Xue, Allicin inhibits osteoblast apoptosis and steroid-induced necrosis of femoral head progression by activating the PI3K/AKT pathway, Food Funct. 11 (9) (2020) 7830–7841.
[46] J.Y. Ho, F.W. Chang, F.S. Huang, J.M. Liu, Y.P. Liu, S.P. Chen, Y.L. Liu, K.C. Cheng, C.P. Yu, R.J. Hsu, Estrogen enhances the cell viability and motility of breast cancer cells through the ERα-ΔNp63-integrin β4 signaling pathway, PLoS One 11 (2) (2016), e0148301.
[47] W. Zhang, C. Qian, S. Li, Protective effect of SGK1 in rat hippocampal neurons subjected to ischemia reperfusion, Cell. Physiol. Biochem. 34 (2) (2014) 299–312.
[48] H. Fan, H.-B. Tang, L.-Q. Shan, S.-C. Liu, D.-G. Huang, X. Chen, Z. Chen, M. Yang, X.-H. Yin, H. Yang, Quercetin prevents necroptosis of oligodendrocytes by inhibiting macrophages/microglia polarization to M1 phenotype after spinal cord injury in rats, J. Neuroinflammation 16 (1) (2019) 1–15.
[49] J.-W. Kim, C. Mahapatra, J.-Y. Hong, M.S. Kim, K.W. Leong, H.-W. Kim, J.K. Hyun, Functional recovery of contused spinal cord in rat with the injection of optimal-dosed cerium oxide nanoparticles, Adv. Sci. (Weinh) 4 (10) (2017) 1700034.
[50] J.-p. Pei, L.-h. Fan, K. Nan, J. Li, X.-q. Dang, K.-z. Wang, HSYA alleviates secondary neuronal death through attenuating oxidative stress, inflammatory response, and neural apoptosis in SD rat spinal cord compression injury, J. Neuroinflammation 14 (1) (2017) 97.
[51] B. Wang, S. Han, Inhibition of inducible nitric oxide synthase attenuates deficits in synaptic plasticity and brain functions following traumatic brain injury, Cerebellum 17 (4) (2018) 477–484.
[52] J. Liu, D.A. Sonshine, S. Shervani, R.H. Hurt, Controlled release of biologically active silver from nanosilver surfaces, ACS Nano 4 (11) (2010) 6903–6913.
[53] Y.S. Kim, J.S. Kim, H.S. Cho, D.S. Rha, J.M. Kim, J.D. Park, B.S. Choi, R. Lim, H.K. Chang, Y.H. Chung, I.H. Kwon, J. Jeong, B.S. Han, Yu, Twenty-eight-day oral toxicity, genotoxicity, and gender-related tissue distribution of silver nanoparticles in sprague-dawley rats, Inhal. Toxicol. 20 (6) (2008) 575–583.
[54] M. van der Zande, R.J. Vandebriel, E. Van Doren, E. Kramer, Z. Herrera Rivera, C.S. Serrano-Rojero, E.R. Gremmer, J. Mast, R.J. Peters, P.C. Hollman, Distribution, elimination, and toxicity of silver nanoparticles and silver ions in rats after 28-day oral exposure, ACS Nano 6 (8) (2012) 7427–7442.